

VALIDATION OF EULERIAN MULTIPHASE FLOW MODELS FOR NUCLEAR SAFETY APPLICATIONS

Thomas Frank*, Junmei Shi^o, Alan D. Burns**

*ANSYS Germany, Staudenfeldweg 12, D-83624 Otterfing, Germany, Thomas.Frank@ansys.com,
^oFZR, Institute of Safety Research, Bautzener Landstr. 128, D-01328 Dresden, Germany, J.Shi@fz-rossendorf.de,
**ANSYS CFX, The Gemini Bldg., Fermi Avenue, Didcot, OX11 0QR, UK, Alan.Burns@ansys.com

ABSTRACT

The CFD package CFX-5 has been used to predict the development of upward directed gas-liquid flows in a vertical pipe. Under the assumption of monodisperse bubbles the dilute gas-liquid flow has been predicted using the Eulerian framework of multiphase flow modeling. The capabilities of the CFX-5 flow solver have been extended by taking into account additional non-drag forces like lift, turbulent dispersion and wall lubrication forces. Range of applicability and accuracy of the numerical model have been validated against measured gas void fraction profiles obtained at the MT-Loop test facility of the Forschungszentrum Rossendorf (FZR) in the bubbly flow regime. Best agreement of numerical results with experimental data could be obtained for a wide range of experimental conditions, if Menter's $k-\omega$ Shear Stress Transport (SST) turbulence model has been used in combination with the Favre averaged drag (FAD) turbulent dispersion force model as derived by Burns et al. [1]. Furthermore results of extensive numerical experiments [2] for the examination and comparison of different model formulations for the wall lubrication and turbulent dispersion forces are presented in this paper.

INTRODUCTION

Prediction of multiphase flows in the field of design, optimization and safety analysis of chemical and nuclear plants requires detailed knowledge of the different flow regimes in gas-liquid multiphase flows and the mechanisms of mass, momentum and heat transfer between the gaseous and liquid phases. So the development of gas void fraction distributions in disperse bubbly flows depends not only on the bubble drag, but also on transverse lift, turbulent dispersion, bubble-wall interaction and bubble induced turbulence. For higher gas volume flow rates the mathematical description of bubble size distribution, bubble breakup and coalescence in dependence on the local flow properties becomes of crucial importance for the description of the main flow phenomena.

The emphasis of this paper is the further development of the multiphase flow models for disperse bubbly flows in the commercial CFD package CFX-5. Due to the necessity to model many of the unresolved details of technical flows in an Eulerian framework of modeling, it is further necessary to assess the accuracy of the CFD method with the help of experimental data. Results for gas void fraction distribution from wiremesh sensor measurements in a vertical pipe bubbly flow at the MT Loop test facility at the Forschungszentrum Rossendorf (FZR) are used to validate the range of applicability and the accuracy of the implemented models.

OUTLINE OF THE PHYSICAL MODEL

Governing equations and CFX-5 two-fluid model

The numerical simulations presented in this work are based on the CFX-5.6 two-fluid (or multifluid) Euler-Euler approach. The Eulerian modeling framework is based on ensemble-averaged mass and momentum transport equations

for all phases. Regarding the liquid phase as continuum ($\alpha=L$) and the gaseous phase (bubbles) as disperse phase ($\alpha=G$) with a constant bubble diameter d_p these equations without mass transfer between phases read:

$$\frac{\partial}{\partial t}(r_\alpha \rho_\alpha) + \nabla \cdot (r_\alpha \rho_\alpha \bar{U}_\alpha) = 0 \quad (1)$$

$$\begin{aligned} & \frac{\partial}{\partial t}(r_\alpha \rho_\alpha \bar{U}_\alpha) + \nabla \cdot (r_\alpha \rho_\alpha \bar{U}_\alpha \otimes \bar{U}_\alpha) \\ & = \nabla \cdot (r_\alpha \mu_\alpha (\nabla \bar{U}_\alpha + (\nabla \bar{U}_\alpha)^T)) - r_\alpha \nabla p \\ & + r_\alpha \rho_\alpha \bar{g} + \bar{F}_D + \bar{M}_\alpha \end{aligned} \quad (2)$$

where M_α represents the sum of interfacial forces besides the drag force F_D , like lift force F_L , wall lubrication force F_{WL} and turbulent dispersion force F_{TD} . For the steady state investigations within the scope of this paper it had been proven that the virtual mass force F_{VM} is small in comparison with the other non-drag forces and therefore it can be safely neglected. Turbulence of the liquid phase has been modeled using either a standard $k-\epsilon$ model or Menter's $k-\omega$ Shear Stress Transport (SST) model [5]. The turbulence of the disperse bubbly phase was modeled using a zero equation turbulence model and bubble induced turbulence has been taken into account according to Sato [6]. The drag force between the bubbles and the fluid was considered in the distorted bubble regime according to the Grace drag model build into CFX-5 [7].

Modeling of non-drag forces

The lift force. The void fraction distribution in gas-liquid two-phase flows is not only determined by the drag force but

is mainly influenced by the so-called ‘non-drag forces’. In vertical pipe flows the main contribution of the non-drag forces is directed perpendicular to the flow direction or pipe axis. So the transversal lift force acting on a spherical particle due to fluid velocity shear can be expressed as:

$$\vec{F}_L = C_L r_G \rho_L (\vec{U}_L - \vec{U}_G) \times \nabla \times \vec{U}_L \quad (3)$$

For solid spherical particles the lift force coefficient C_L is usually positive and can be determined in dependency on the particle Reynolds number and a dimensionless shear rate parameter. Corresponding correlations had been published by Saffman (1965/68), McLaughlin (1991/93), Dandy & Dwyer (1990), Mei, Adrian & Klausner (1991/92/94), Legendre & Magnaudet (1998) and Tomiyama (1998) (see [11, 12]). In the works of Tomiyama (1998) and Moraga et al. (1999) negative values for the lift force coefficient for bubbles and spherical solid particles were reported. The correlation given by Moraga et al. was based on experimental data of Alajbegovic et al. (1994) and was explained by superposition of inviscid aerodynamic and vortex-shedding induced lift forces resulting in a sign change of the lift force with increasing particle Reynolds number and shear rate. Similarly for bubbles with a larger bubble diameter, bubble deformation and asymmetric wake effects become of importance, so that the lift force coefficient C_L becomes negative. A correlation for C_L as a function of the bubble Eötvös number was published by Tomiyama (1998) [8]. This correlation has been used here in a slightly modified form, where the value of C_L for $EO_d > 10$ has been changed to $C_L = -0.27$ to ensure a steady dependency of $C_L = C_L(EO_d)$:

$$C_L = \begin{cases} \min[0.288 \tanh(0.121 Re_p), f(EO_d)], & EO_d < 4 \\ f(EO_d), & 4 \leq EO_d \leq 10 \\ -0.27, & EO_d > 10 \end{cases} \quad (4)$$

with:

$$f(EO_d) = 0.00105 EO_d^3 - 0.0159 EO_d^2 - 0.0204 EO_d + 0.474 \quad (5)$$

where EO_d is the Eötvös number based on the long axis d_H of a deformable bubble, i.e.:

$$EO_d = \frac{g(\rho_L - \rho_G) d_H^2}{\sigma}, \quad d_H = d_p (1 + 0.163 EO)^{1/3} \quad (6)$$

$$EO = \frac{g(\rho_L - \rho_G) d_p^2}{\sigma}$$

The wall lubrication force. Antal et al. (1991) [9] proposed an additional wall lubrication force to model the repulsive force of a wall on a bubble, which is caused by the asymmetric fluid flow around bubbles in the vicinity of the wall due to the fluid boundary layer:

$$\vec{F}_{WL} = -C_{WL} r_G \rho_L \left| \vec{U}_{rel} - (\vec{U}_{rel} \cdot \vec{n}_W) \vec{n}_W \right|^2 \vec{n}_W \quad (7)$$

with:

$$C_{WL} = \max \left\{ 0, \frac{C_{W1}}{d_p} + \frac{C_{W2}}{y_w} \right\} \quad (8)$$

The authors recommended coefficient values of $C_{W1} = -0.01$ and $C_{W2} = 0.05$. However the coefficients determined by Krepper et al. [10] for the investigated test geometry were $C_{W1} = -0.0064$ and $C_{W2} = 0.05$. Tomiyama [8] has modified the wall lubrication force formulation of Antal based on experiments with air bubbles in glycerin:

$$C_{WL} = C_{W3} \frac{d_p}{2} \left(\frac{1}{y_w^2} - \frac{1}{(D - y_w)^2} \right) \quad (9)$$

where the coefficient C_{W3} is dependent on the Eötvös number for deformable bubbles. Again due to the assumption of a steady dependency of $C_{W3} = C_{W3}(EO)$ we use a slightly changed expression for this wall lubrication coefficient:

$$C_{W3} = \begin{cases} e^{-0.933 EO + 0.179} & 1 \leq EO \leq 5 \\ 0.00599 EO - 0.0187 & 5 < EO \leq 33 \\ 0.179 & 33 < EO \end{cases} \quad (10)$$

The turbulent dispersion force. Initially a simple formulation of the turbulent dispersion force was proposed by Lopez de Bertodano et al. [13] from the Rensselaer Polytechnic Institute (RPI):

$$\vec{F}_{TD} = -C_{TD} \rho_L k_L \nabla r_G \quad (11)$$

where different constant values for the turbulent dispersion force coefficient of $C_{TD} = 0.1, \dots, 0.5$ have been used by many authors. This model will be further referenced to as the RPI TD model. Several other models had appeared in the literature (see [13]), notably those of Carrica [14] and Gosman & Issa [15,16], which had shown that the turbulent dispersion coefficient C_{TD} is in fact a function of the Stokes number and other flow properties. Recently Burns et al. [1] published a mathematical derivation for the turbulent dispersion force based on a second time averaging process applied to the drag term in the momentum transport equations of Eulerian multiphase flow modeling, since the physical mechanism responsible for turbulent dispersion is the action of turbulent eddies via interphase drag.

$$F_{D,\alpha} = D_{\alpha\beta} A_{\alpha\beta} (U_\beta - U_\alpha)$$

$$\overline{F_{D,\alpha}} = D_{\alpha\beta} (\overline{A_{\alpha\beta}} (\overline{U_\beta} - \overline{U_\alpha}) + \overline{a'_{\alpha\beta}} (\overline{u'_\beta} - \overline{u'_\alpha})) \quad (12)$$

Here the interphase drag is expressed via interfacial area density $A_{\alpha\beta}$ and a coefficient $D_{\alpha\beta}$. If the time averaged drag term is expressed in terms of so-called Favre or mass-weighted averaged velocities:

$$\tilde{U}_\alpha = \overline{U_\alpha} + \frac{\overline{r'_\alpha u'_\alpha}}{r_\alpha} \quad (13)$$

we obtain from eq. (12):

$$\begin{aligned} \overline{F_{D,\alpha}} &= D_{\alpha\beta} \overline{A_{\alpha\beta}} (\tilde{U}_\beta - \tilde{U}_\alpha) \\ &+ D_{\alpha\beta} \overline{A_{\alpha\beta}} \left(\frac{r'_\alpha u'_\alpha}{r_\alpha} - \frac{r'_\beta u'_\beta}{r_\beta} + \frac{a'_{\alpha\beta} (u'_\beta - u'_\alpha)}{A_{\alpha\beta}} \right) \end{aligned} \quad (14)$$

Regarding the first term as the drag term expressed in Favre averaged variables we obtain an expression for the turbulent dispersion force from the additional correlation terms in eq. (14). In case of dilute dispersed multi-phase flow, the turbulent dispersion force term can be further simplified using the following expression for interfacial area density and eddy diffusivity hypothesis:

$$A_{\alpha\beta} = \frac{6r_\beta}{d_\beta}, \quad \overline{r'_\alpha u'_\alpha} = -\frac{v_{t\alpha}}{\sigma_{r\alpha}} \nabla \overline{r_\alpha} \quad (15)$$

where $\sigma_{r\alpha}$ is a turbulent Schmidt number for volume fraction dispersion, expected to be in the order of unity. In that case we finally obtain for the turbulent dispersion force in Favre averaged momentum transport equations:

$$\overline{F_{TD,\alpha}} = D_{\alpha\beta} \overline{A_{\alpha\beta}} \frac{v_{t\alpha}}{\sigma_{r\alpha}} \left(\frac{\nabla \overline{r_\beta}}{r_\beta} - \frac{\nabla \overline{r_\alpha}}{r_\alpha} \right) \quad (16)$$

This model will be further referenced to as the Favre Averaged Drag (FAD) TD model. Comparing expression from eq. (16) for disperse two-phase flows with the expression for F_{TD} from the RPI TD model in eq. (11), we see that the two models are equivalent if the turbulent dispersion force coefficient C_{TD} of the RPI TD model is set to:

$$\begin{aligned} C_{TD} &= \frac{C_\mu}{\sigma_{r\alpha}} \frac{D_{\alpha\beta} A_{\alpha\beta} k_\alpha}{\rho_\alpha \varepsilon_\alpha} \left(\frac{1}{r_\alpha} + \frac{1}{r_\beta} \right) \\ &= \frac{3}{4} C_D \frac{v_{tL}}{\sigma_{rL}} \frac{|U_L - U_G|}{d_p k_L} \frac{1}{1 - r_G} \end{aligned} \quad (17)$$

It will be shown from the numerical simulations, that the variation in the value of the turbulent dispersion force coefficient C_{TD} in the FAD TD model is large in comparison with the assumed constant values for C_{TD} from the RPI TD model in eq. (11) and that it can not be neglected for disperse bubbly flows.

CFX-5 NUMERICAL SIMULATIONS AND COMPARISON WITH EXPERIMENTAL DATA

Experiments and void fraction profile data

Numerical simulation data has been validated against extensive experimental results for air-water bubbly flows available from a FZR database [3, 4]. The measurements at the MT-Loop test facility (Fig. 1) were carried out at a vertical test section of 4m height and 51.2mm inner diameter. Air bubbles were injected into an upward water flow at normal conditions using a sparger with 19 capillaries equally

distributed over the pipe cross section. A large number of tests with different ratios of air and water superficial velocities resulting in a slightly varying bubble diameter were performed (Tab. 1). In the tests used for the current validation the loop was operated with air at atmospheric pressure and 30°C temperature. Stationary conditions were settled for each experiment. Gas void fraction profiles were measured at a height of 3.08m above the air injection using a fast wiremesh sensor developed at FZR [3] with 24x24 electrodes. Additionally bubble size and void fraction distributions are available for 10 different measurement cross sections at different L/D=0.6,...,59.2.

Tab. 1: Test conditions for experimental investigations at the MT-Loop test facility

FZR Test No.	\bar{d}_p [mm]	$U_{L,sup}$ [m/s]	$U_{G,sup}$ [m/s]
017	4.8	0.405	0.0040
019	4.8	1.017	0.0040
038	4.3	0.225	0.0096
039	4.5	0.405	0.0096
040	4.6	0.641	0.0096
041	4.5	1.017	0.0096
042	3.6	1.611	0.0096
074	4.5	1.017	0.0368

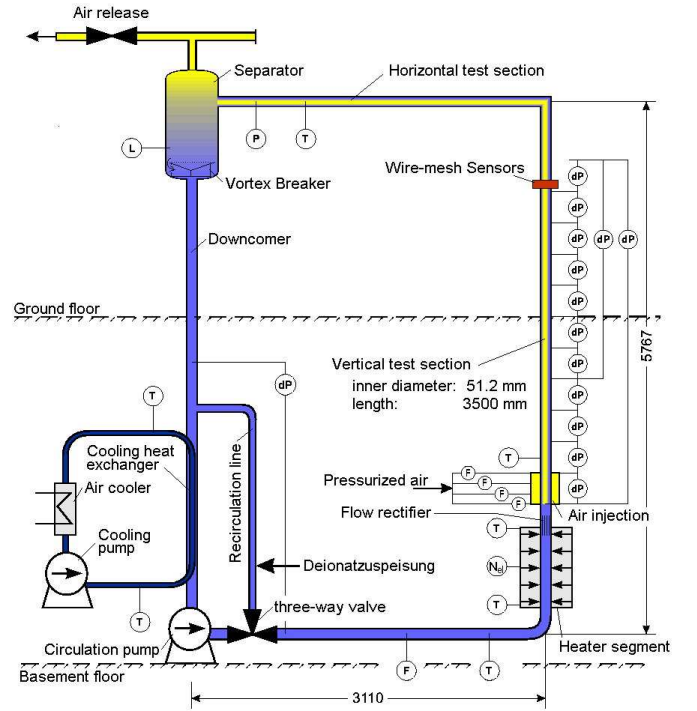


Fig. 1: MT-Loop test facility for vertical pipe flow investigations

Setup of the numerical simulation

Extensive numerical simulations for the different test cases from Tab. 1 had been carried out in order to validate the previously discussed non-drag force models. Therefore the lift, wall lubrication and turbulent dispersion forces in accordance to the eq. (3), (4), (7), (8), (9), (16) and (17) were implemented into CFX-5.6 using User Fortran routines or CCL command language expressions.

The numerical simulations had been carried out in accordance with the Best Practice Guidelines for CFD code validation [17]. For the vertical pipe flow geometry shown in

Fig. 1 radial symmetry has been assumed, so that the numerical simulations could be performed on a 60° radial sector of the pipe with symmetry boundary conditions at both sides. Inlet conditions were assumed to be homogeneous in terms of superficial liquid and gas velocities and volume fractions for both phases in accordance with the experimental setup conditions from Tab. 1. For the disperse bubbly phase a mean bubble diameter was specified, which was determined from the test case wiremesh sensor data. At the outlet cross section of the 3.8m long pipe section an averaged static pressure outlet boundary condition was used.

Tab. 2: Hierarchy of numerical meshes

Grid level	No. of CV's in pipe cross section	No. of CV's along pipe axis	No. of CV's
1	192	82	15 744
2	320	100	32 000
3	500	128	64 000
4	819	158	129 402
5	1 280	200	256 000

A hierarchy of 5 numerical grids was constructed, where the number of grid elements has been increased by a factor of 2 from a coarser to a finer mesh (scaling factor of $2^{1/3}$ in each coordinate direction, see Tab. 2). The numerical meshes used local refinement towards the outer pipe wall, while min/max cell size and cell aspect ratios were kept almost constant for all different numerical grids. Dimensionless y^+ values varied between $y^+=29.2$ on the coarsest mesh and $y^+=12.5$ on the finest mesh.

For investigation of flow solver convergence the gas holdup and the global mass balances for both phases in the vertical pipe were defined as monitored target variables. Reliable converged solutions could be obtained on all grid levels for a satisfied convergence criterion based on the maximum residuals of $1.0e-5$ and for a physical time scale of the fully implicit solution method of $\Delta t=0.005s$.

Numerical simulation vs. Experiment

For the comparison of the numerically predicted and measured gas volume fraction profiles at the uppermost measurement cross section at $z=3.03m$ ($L/D=59.2$) all data have been normalized:

$$r_G^*(x) = \frac{r_G(x)}{\frac{8}{D^2} \int_0^{D/2} r_G(x) x dx} \quad (18)$$

where x is the coordinate in radial direction.

In a first series of numerical simulations the dependency of the gas void fraction distribution on the fluid phase turbulence model (standard $k-\epsilon$ vs. SST model) and the turbulent dispersion force model (RPI vs. FAD TD model) has been investigated for test case FZR-074. Additionally the Tomiyama lift and wall lubrication forces have been taken into account. Fig. 2 shows the comparison of the gas void fraction profiles for the 2nd grid level with the experimental result. It can be observed, that the Tomiyama lift and wall lubrication forces are well balanced and give a pronounced wall peak in the gas void fraction profile, which is the expected void fraction distribution for the given bubble diameter in this test case. On the other hand this wall peak is much too pronounced in comparison with the experimental

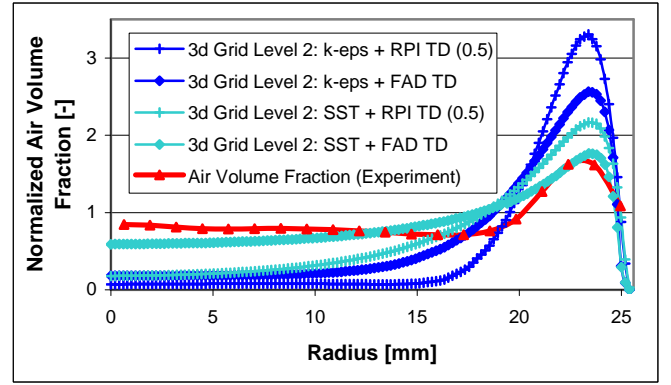


Fig. 2: Comparison of void fraction profiles for test case FZR-074

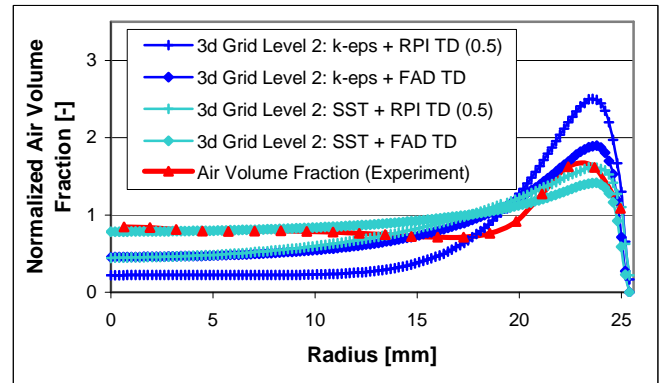


Fig. 3: Void fraction profiles using reduced Tomiyama's lift and wall lubrication forces (FZR-074)

data for the simulations using the standard $k-\epsilon$ turbulence model. Furthermore the turbulent dispersion of the disperse phase is underpredicted with the RPI TD model also resulting in too high gas void fraction values in the wall peak. Best results could be obtained with the combination of the SST turbulence model for the continuous phase using automatic wall function treatment [5, 7] and the FAD TD model for the disperse phase. The higher turbulent dispersion of the FAD TD model leads not only to better agreement of void fraction data within the region of the wall peak but leads also to a substantial improvement of the void fraction distribution near the pipe axis.

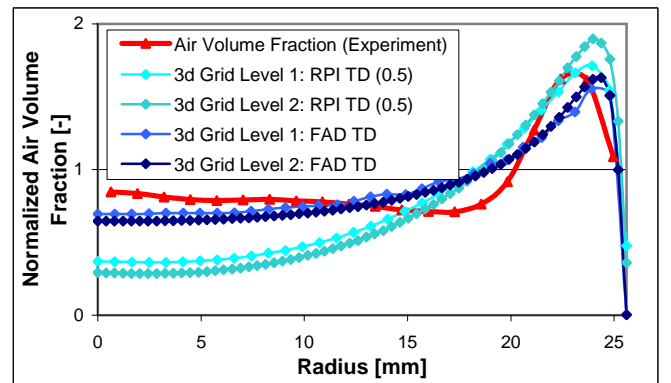


Fig. 4: Comparison of RPI vs. FAD TD model for test case FZR-074 with Tomiyama lift and Antal's wall lubrication forces and Sato model

Since in Fig. 2 the numerically predicted level of the void fraction profile in the pipe core is still less than the experimentally measured value it could be suggested, that the

Tomiyama lift force predicts too high positive values, which are not well balanced with the turbulent dispersion force in that core region. Therefore an analogous numerical experiment has been carried out by reducing the amplitude of the Tomiyama lift and wall lubrication forces by a factor of 0.5. Results for the radial gas void fraction distribution in Fig. 3 show the same trends as discussed for the previous series of numerical simulations. Again the combination of the SST turbulence model with the FAD model for the turbulent dispersion force delivers the best agreement with the experimental result. With the reduced lift and wall lubrication forces the agreement in the pipe core region is very good, while the maximum amplitude of the wall peak in the gas volume fraction is slightly below the measured value.

A similar numerical investigation had been carried out using the Tomiyama lift and Antal's wall lubrication forces with the SST turbulence and Sato models on two different grid levels of refinement. Fig. 4 shows, that again the RPI TD model underpredicts the turbulent dispersion in the pipe core leading to higher amplitude of the peak in the gas volume fraction distribution near the wall. Additionally with Antal's wall lubrication force the radial location of the wall peak is predicted to close to the wall in comparison with experimental results.

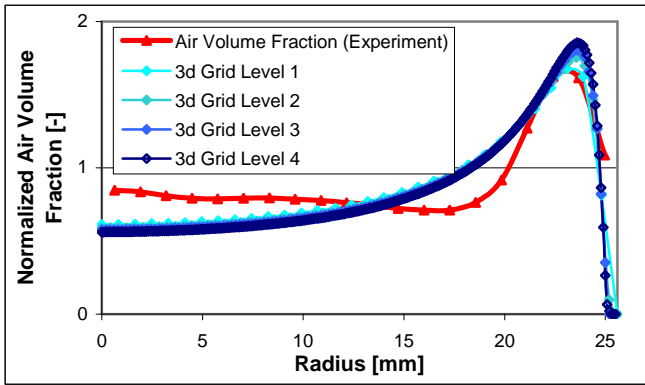


Fig. 5: Grid independence of numerical results: FZR-074 with Tomiyama lift and Tomiyama wall lubrication forces, FAD TD and Sato model

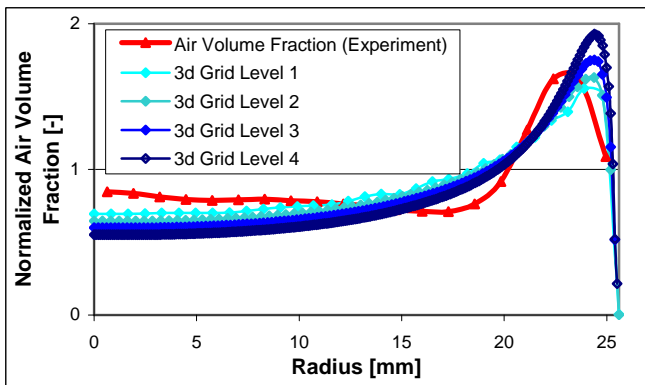


Fig. 6: Grid independence of numerical results: FZR-074 with Tomiyama lift and Antal's wall lubrication forces, FAD TD and Sato model

It has further to be mentioned, that the gradient of the gas void fraction in the turbulent dispersion force term can lead to numerical node-to-node oscillations, if central differences are used for the discretization of this term. These oscillations can be avoided by inclusion of the turbulent dispersion force in a coupling algorithm similar to the algorithm developed by Rhie

& Chow for suppression of pressure fluctuations on colocated grids.

Furthermore, the grid dependence of the numerical results has been studied. Figs. 5 and 6 show the corresponding gas void fraction profiles in comparison with the experimental data for grid levels 1 to 4 using either Tomiyama's or Antal's wall lubrication force formulation. In Fig. 5 numerical simulations give almost grid independent results for grid resolutions finer than the 2nd grid level, when Tomiyama's wall lubrication force formulation has been used. For the case with Antal's wall lubrication (Fig. 6), grid independent results could not be obtained even on the 4th grid level. On grids with finer grid resolution the misbalance between Antal's wall lubrication force and Tomiyama's lift force leads to increasing amplitude of the wall peak in the gas volume fraction distribution, while the radial location of the void fraction maximum remains unchanged. Again the radial shift of the void fraction peak towards the wall can be observed in Fig. 5 in comparison with the obtained void fraction distributions from Figs. 2-3 and 5. This indicates, that the wall lubrication force derived from Antal's formulation seems too weak in order to balance Tomiyama's lift force at the correct radial location, so that the disperse phase is too much accumulated within a certain number of grid cells near the wall.

Nevertheless Figs. 4-6 show again, that the use of the FAD TD model leads to a significant improvement in the agreement of the numerical results with the experimental void fraction data, especially regarding the higher gas void fraction values in the pipe core and the maximum amplitude of the wall peak in the gas void fraction profiles. With the constant coefficient RPI TD model the near-wall void fraction peak in the gas volume fraction distribution is overpredicted in all cases due to a reduced turbulent dispersion force. Consequently high concentration of the disperse phase near the wall leads to large errors in the gas void fraction level in the pipe core by using the RPI TD model.

Further Figs. 7-10 show the distribution of the lift and wall lubrication forces in the cross section at $z=3.03\text{m}$ ($L/D=59.2$) for the following four different simulations and for the grid levels 1-4:

- Tomiyama lift (1.0), Antal's wall lubrication and RPI turbulent dispersion forces ($C_{TD}=0.5$);
- Tomiyama lift (1.0), Antal's wall lubrication and FAD turbulent dispersion forces;
- Tomiyama lift (1.0), Tomiyama wall lubrication (1.0) and FAD turbulent dispersion forces;
- reduced Tomiyama lift (0.5), reduced Tomiyama wall lubrication (0.5) and FAD turbulent dispersion forces.

It can be observed, that for the cases (a) and (b) the lift and wall lubrication forces reach their highest values very close to the wall, on 1st-3rd grid levels even within the wall nearest grid cell. Otherwise in cases (c) and (d) a force balance between the Tomiyama lift and wall lubrication forces can be established at a certain grid independent wall distance. In the simulations where Antal's wall lubrication force was used, a similar balance of the non-drag forces is not established up to the grid cell closest to the wall. In combination with the RPI TD model this had led even to numerical instabilities in the numerical solutions on grid levels 3 and 4.

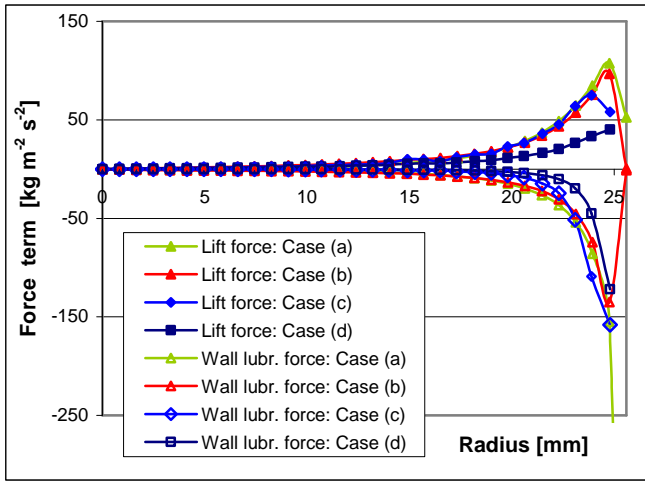


Fig. 7: Distribution of non-drag force terms on 1st grid level (FZR-074)

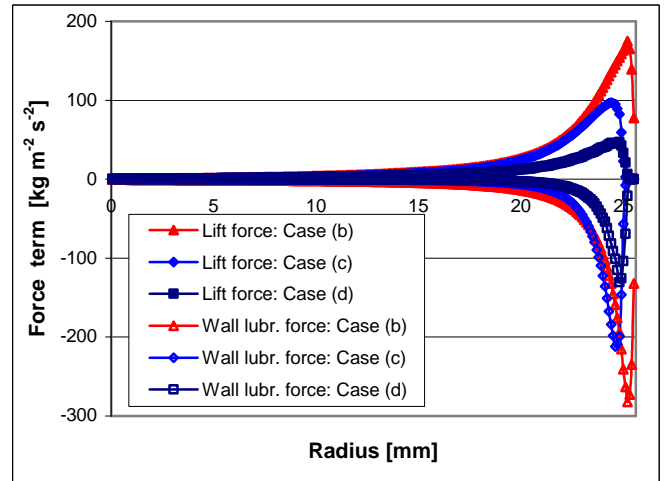


Fig. 10: Distribution of non-drag force terms on 4th grid level (FZR-074)

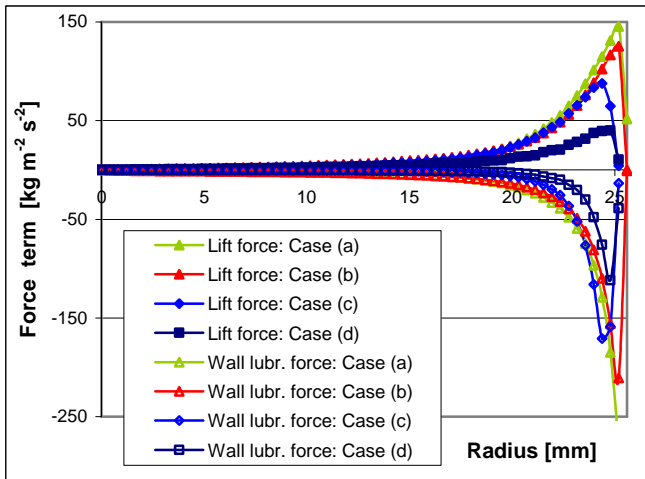


Fig. 8: Distribution of non-drag force terms on 2nd grid level (FZR-074)

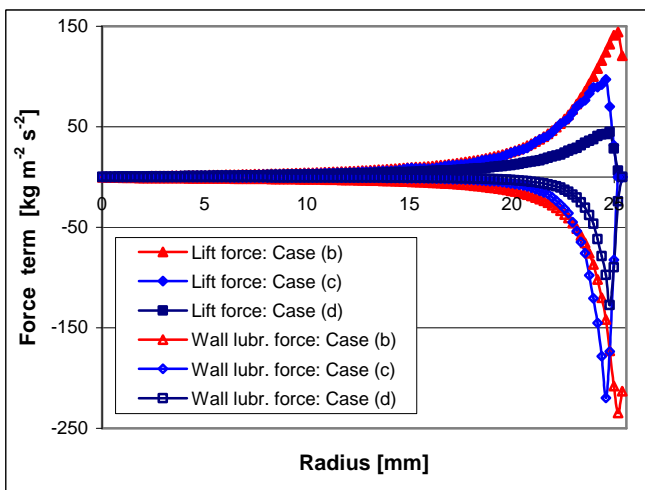


Fig. 9: Distribution of non-drag force terms on 3rd grid level (FZR-074)

Finally the physical setup with the implementation of the Tomiyama lift and wall lubrication forces and the FAD TD force model was applied to different flow conditions defined by the experimental setup given in Tab. 1 for the test cases FZR-038 to FZR-042. For computational efficiency these simulations were carried out using two-dimensional grids considering the axi-symmetrical geometry. Again careful grid dependence studies were carried out. The final grid independent results were obtained on 2d grids with 35x600 control volumes and with radial near wall refinement of grid cells.

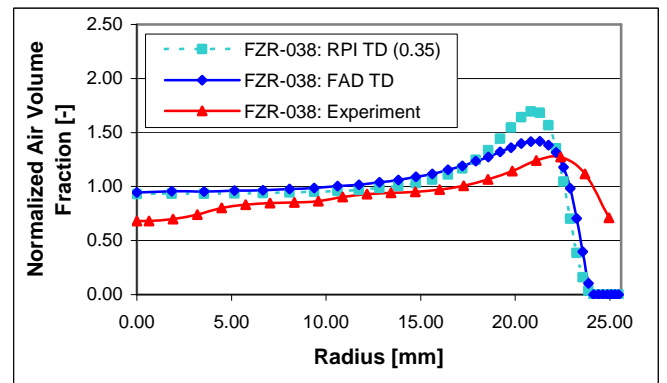


Fig. 11: Comparison of numerical simulation vs. experimental results for FZR-038

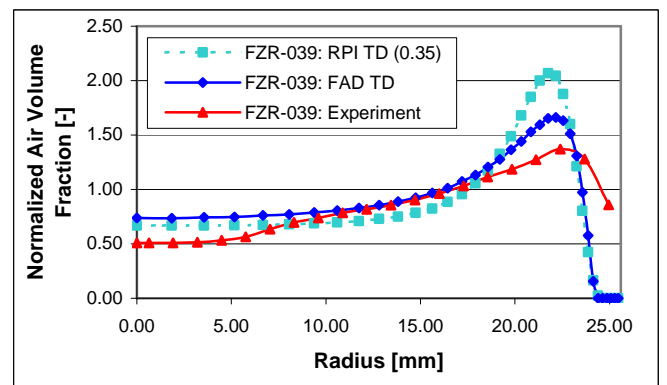


Fig. 12: Comparison of numerical simulation vs. experimental results for FZR-039

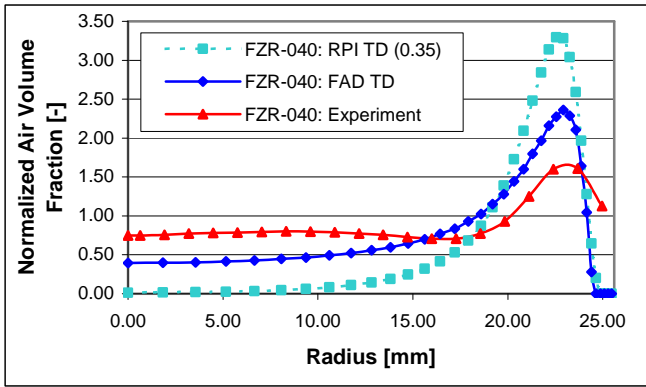


Fig. 13: Comparison of numerical simulation vs. experimental results for FZR-040

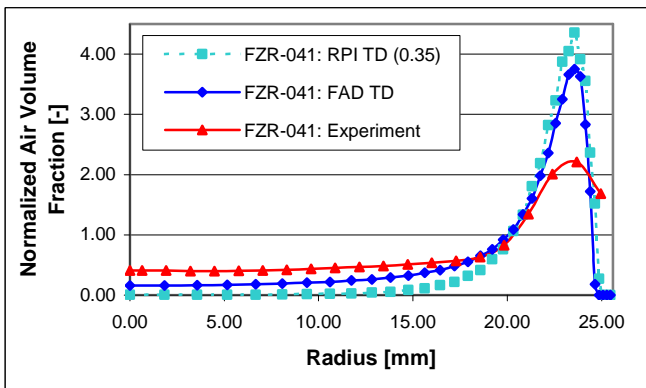


Fig. 14: Comparison of numerical simulation vs. experimental results for FZR-041

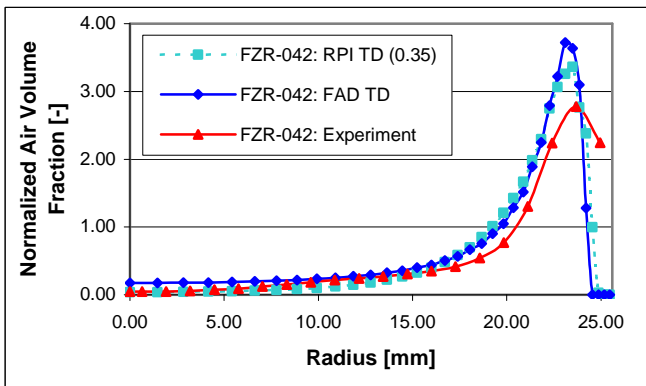


Fig. 15: Comparison of numerical simulation vs. experimental results for FZR-042

For comparison, the simulations were also carried out with the RPI TD model and $C_{TD}=0.35$. Results of these test case predictions are presented in Figs. 11-15 and compared with the experimentally measured gas void fraction profiles. It can be observed that the agreement between numerical simulation and experimental results are fairly good, if the several sources of uncertainties are taken into account. These uncertainties include temperature, phase change (certain amount of evaporation) and compressible effects (hydrostatic bubble expansion) on void fraction, breakup and coalescence phenomena, which had not yet been taken into account in the numerical simulations, the constants of experimental conditions and possible measurement accuracy.

Figs. 11-15 show the change in gas volume fraction profiles from a nearly uniform void fraction distribution with only a weak wall peak (FZR-038) to a strong concentration of

the disperse bubbly phase in a pronounced wall peak of the void fraction (FZR-042). This change in gas void fraction distribution with increased superficial water velocity and decreased ratio of air to water volume flow rate can be well predicted with the implemented physical models. In the intermediate range (FZR-040/041) both the RPI and the FAD TD models still underpredict the near wall turbulent dispersion resulting in an overprediction of near wall gas volume fractions. Furthermore the Tomiyama wall lubrication model leads to a thin bubble free region near the wall, while measurement data still detect a significant level of air void fraction in this region. Nevertheless, the reduced accuracy of the wire mesh sensor measurement close to the pipe wall is also at least partially responsible for this discrepancy.

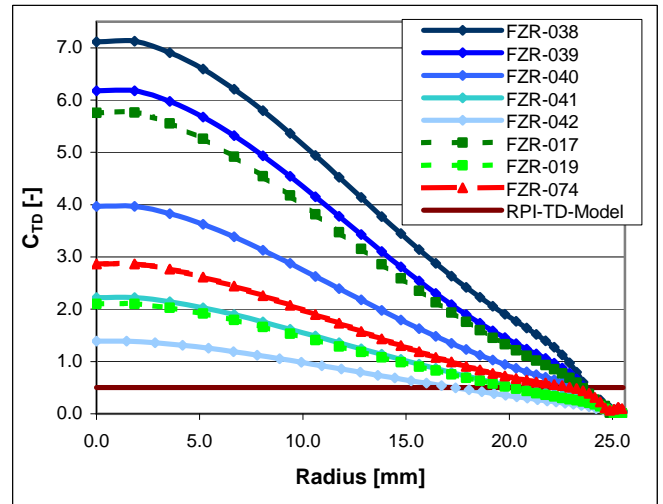


Fig. 16: Turbulent dispersion force coefficient C_{TD} vs. pipe radius

If for the above numerical simulations the turbulent dispersion force coefficient C_{TD} from eq. (17) is plotted over the pipe radius and compared with the recommended constant value of $C_{TD}=0.5$ for the RPI TD model, we can see the strong difference in the predicted turbulent dispersion force of the FAD TD model (see Fig. 16). Especially in the core of the gas-liquid bubbly pipe flow the turbulent dispersion force coefficient C_{TD} in the FAD TD model shows a strong increase in comparison with the value commonly used with the RPI TD model. Furthermore it can be observed, that the overall values of the C_{TD} coefficient decrease with increasing superficial liquid velocity $U_{L,sup}$ or Reynolds number.

SUMMARY & CONCLUSIONS

Consideration of the lift, wall lubrication and turbulent dispersion forces in the multiphase momentum equations is essential for the modeling of gas-liquid bubbly pipe flows or of even greater importance in more complex flow situations. The multiphase flow capabilities of the CFX-5 flow solver have been enhanced by implementation of some of the most widely used models for the additional non-drag force terms. Additionally the Favre Averaged Drag (FAD) turbulent dispersion model in its formulation derived by Burns [1] has been implemented and successfully validated against experimental data for the radial gas volume fraction distribution from the MT-Loop test facility at Forschungszentrum Rossendorf (FZR). Validation tests have shown, that dilute gas-liquid bubbly flows with a monodispersed bubble

size distribution can successfully be predicted with the multiphase models of CFX-5. In dependence on the bubble diameter either a near wall peak or a core peak in the gas void fraction profiles of vertically upward directed pipe flow has been determined in accordance with the experimental results. Best agreement with the experimental data has been established using the SST turbulence model with automatic wall treatment for the liquid phase turbulence modeling, the Tomiyama lift and wall lubrication force models together with the FAD turbulent dispersion force model for the disperse phase.

Further development is necessary for bubbly flows of higher gas void fraction taking into account bubble breakup and coalescence together with the different velocities of disperse phases with different bubble sizes in a framework of multi-fluid Eulerian modeling.

ACKNOWLEDGEMENT

This research was carried out in strong cooperation between ANSYS and the Forschungszentrum Rossendorf (FZR), Germany. Further this research was supported by the German Ministry of Economy and Labour (BMWA) in the framework of the GRS-BMWA network project CFD-Verbundvorhaben "Entwicklung von CFD-Software zur Simulation mehrdimensionaler Strömungen in der Reaktorsicherheit"¹ and in the project "TOPFLOW - Transient Two Phase Flow Test Facility for generic investigation of Two Phase Flows and further Development and Validation of CFD Codes".

NOMENCLATURE

$A_{\alpha\beta}$ [1/m]	- interfacial area density
C_L [-]	- lift force coefficient
C_{TD} [-]	- turbulent dispersion force coefficient
C_{WL} [-]	- wall lubrication force coefficient
C_μ [-]	- turbulence model constant
d_H [m]	- long axis of a deformable bubble
d_p [m]	- bubble diameter
D [m]	- pipe diameter
$Eo = \frac{g(\rho_L - \rho_G)d_p^2}{\sigma}$ [-]	- Eötvös number
k [m ² /s ²]	- turbulence kinetic energy
L [m]	- pipe length
\vec{n}_w [-]	- wall normal vector
p [Pa]	- pressure
r [-]	- void fraction
$Re_p = \frac{\rho_L U_L - U_G d_p}{\mu_L}$ [-]	- particle Reynolds number
U [m/s]	- velocity
$U_{rel} = U_L - U_G$ [m/s]	- slip velocity
y_w [m]	- wall distance
y^+ [-]	- dimensionless wall distance

Greek symbols

ε [m ² /s ³]	- turbulence eddy dissipation
ρ [kg/m ³]	- density
ν [m ² /s]	- kinematic viscosity
ν_t [m ² /s]	- turbulent viscosity
μ [kg/m s]	- viscosity
σ_r [-]	- Schmidt number
σ [N/m]	- surface tension

Subscripts and superscripts

'	- fluctuation
G	- gaseous phase
L	- liquid phase
sup	- superficial
t	- turbulent
α, β	- indices for continuous and disperse phase in a phase pair

REFERENCES

1. A.D. Burns, Th. Frank, I. Hamill, J.-M. Shi, The Favre Averaged Drag Model for Turbulence Dispersion in Eulerian Multi-Phase Flows, *ICMF'2004, 5th Int. Conf. Multiphase Flow*, Yokohama, Japan, 2004.
2. Th. Frank, F.R. Menter, *Bubble flow in vertical pipes – Investigation of the test case VDL-01/1 for the validation of CFD codes*, ANSYS CFX Germany, Technical Report No. TR-03-09, pp. 34, October 2003.
3. H.-M. Prasser, D. Lucas, E. Krepper, D. Baldauf, A. Böttger, U. Rohde et.al, *Strömungskarten und Modelle für transiente Zweiphasenströmungen*, Forschungszentrum Rossendorf, Germany, Report No. FZR-379, pp. 183, June 2003.
4. D. Lucas, E. Krepper, H.-M. Prasser, Development of bubble size distributions in vertical pipe flow by consideration of radial gas fraction profiles, *ICMF'2001, 4th Int. Conf. Multiphase Flow*, New Orleans, LA, USA, pp. 1-12, June 2001.
5. F.R. Menter, Two-equation eddy-viscosity turbulence models for engineering applications, *AIAA-Journal*, Vol. 32, No. 8, 1994.
6. Y. Sato, K. Sekoguchi, Liquid velocity distribution in two phase bubble flow, *Int. J. Multiphase Flow*, Vol. 2, pp. 79, 1975.
7. CFX-5.6 Users Manual, ANSYS, 2003.
8. A. Tomiyama, Struggle with computational bubble dynamics, *ICMF'98, 3rd Int. Conf. Multiphase Flow*, Lyon, France, pp. 1-18, June 8.-12. 1998.
9. S.P. Antal, R.T. Lahey, J.E. Flaherty, Analysis of phase distribution in fully developed laminar bubbly two-phase flow, *Int. J. Multiphase Flow*, Vol. 7, pp. 635-652, 1991.
10. E. Krepper, H.M. Prasser, Measurements and CFX-Simulations of a bubbly flow in a vertical pipe, *AMIF-ESF Workshop "Computing Methods for Two-Phase Flow"*, Aussois, France, pp. 8, 12-14 January 2000.

¹ CFD network project "Development of CFD codes for multidimensional flows in reactor safety applications"

11. Th. Frank, *A review on advanced Eulerian multiphase flow modeling for gas-liquid flows*, ANSYS CFX Germany, Technical Report No. TR-03-08, pp. 23, March 2003.
12. Th. Frank, *Parallele Algorithmen für die numerische Simulation dreidimensionaler, disperser Mehrphasenströmungen und deren Anwendung in der Verfahrenstechnik*, Berichte aus der Strömungstechnik, Shaker Verlag, Aachen, pp. 328, 2002.
13. F.J. Moraga, A.E. Larreteguy, D.A. Drew, R.T. Lahey, Assessment of turbulent dispersion models for bubbly flows in the low Stokes number limit, *Int. J. Multiphase Flow*, Vol. 29, pp. 655-673, 2003.
14. P.M. Carrica, D.A. Drew, R.T. Lahey, A polydisperse model for bubbly two-phase flow around a surface ship, *Int. J. Multiphase Flow*, Vol. 25, pp. 257-305, 1999.
15. A. Behzadi, R.I. Issa, H. Rusche, Effects of turbulence on inter-phase forces in dispersed flow, *ICMF'2001, 4th Int. Conf. Multiphase Flow*, New Orleans, LA, USA, pp. 1-12, June 2001.
16. A.D. Gosman, C. Lekakou, S. Politis, R.I. Issa, M.K. Looney, Multidimensional modeling of turbulent two-phase flows in stirred vessels, *AIChE Journal*, Vol. 38, No. 12, pp. 1946-1956, December 1992.
17. F.R. Menter, *CFD Best Practice Guidelines (BPG) for CFD code validation for reactor safety applications*, EC Project ECORA, Report EVOL-ECORA-D01, pp. 1-47, 2002.